

The effect of boric acid content on the properties of electrochemically prepared Ni–Fe/ITO thin films

U. Saraç^{a,*}, M. Kaya^b, M. C. Baykul^c

^a*Department of Science Education, Bartın University, 74100, Bartın, Turkey*

^b*Vocational School of Health Service, Eskişehir Osmangazi University, 26480, Eskişehir, Turkey*

^c*Department of Metallurgical and Materials Engineering, Eskişehir Osmangazi University, 26480, Eskişehir, Turkey*

This paper reports the role of the boric acid (H_3BO_3) content in a sulphate based aqueous electrolyte (AE) on the magnetic characteristics, deposit composition, domain structure, surface morphologies and structural properties of the Ni–Fe/ITO thin film samples grown by electrochemical deposition (ED) technique. The results show that the amount of the H_3BO_3 must be controlled to obtain the proper Ni–Fe/ITO thin film samples without brittle properties. The influence of the H_3BO_3 content in the AE on the deposit composition, structural parameters and magnetic characteristics is found to be negligible. However, the roughness parameters and the size of the nodular particles are noticeably influenced by the H_3BO_3 content. All samples have nanosized crystallites in the range of 19.6–20.5 nm. The films possess almost the same magnetic squareness ratio (11 ± 2) and coercivity values (49 ± 1 Oe). In all deposits, regardless of the H_3BO_3 content, quite large magnetic stripe domains with a width of 1.6 ± 0.2 μm are also detected. The films exhibit a uniform surface structure consisting of nodular particles. However, increasing H_3BO_3 content in the AE leads to a dramatic reduction in the width of the surface particles. Furthermore, the surface roughness of the samples considerably decreases as the H_3BO_3 content in the AE is increased.

(Received April 18, 2021; Accepted August 16, 2021)

Keywords: Electroplated Ni–Fe/ITO thin films, Structural properties, Boric acid content, Magnetic characteristics, Surface roughness, Particle size, Stripe domains

1. Introduction

Ferromagnetic Ni–Fe alloys exhibiting nanostructured characteristics have excellent properties such as low coercivity, relatively high permeability, high saturation magnetization and low thermal expansion coefficient [1–9]. These desired features make ferromagnetic Ni–Fe alloys one of the perfect candidates for many industrial and technological applications [1–7, 9, 10]. To produce such metallic thin film systems, several effective process have been reported in the literature as follows: molecular beam epitaxy, sputtering, evaporation and electrochemical deposition (ED) [9]. In this work, ED process without a vacuum was preferred in manufacturing process of the Ni–Fe/ITO alloy thin films. Compared to high–vacuum processes, ED has been widely used in manufacturing process of ferromagnetic single, alloy, composite and multilayer systems at the nanometer scale due to its rapid fabrication time, flexibility, simplicity, versatility, repeatability and economic advantages [1–3, 5, 11–15]. On the other hand, it is well known that the boric acid (H_3BO_3) is a common additive utilized in ED process of a wide variety of materials including iron group elements from both chloride and sulphate based aqueous electrolytes (AEs) [9, 16]. It has been shown that the morphology of the materials prepared by ED technique can be improved, the brittleness of the samples can be reduced and the brighter deposits can be obtained by adding H_3BO_3 to the AE [17–26]. As a buffering chemical agent, the H_3BO_3 can inhibit pH raise on cathode surface and can prevent hydroxide formation [27–29]. Furthermore, the H_3BO_3 can act as a homogeneous catalyst for metal deposition [29–31]. Although H_3BO_3 is a common additive used in the ED process of the Ni–Fe/ITO thin films [11, 32–34], the effect of the H_3BO_3

* Corresponding author: usarac@bartin.edu.tr

content in AE on the electroplated Ni–Fe/ITO thin film samples has not yet been studied. Moreover, most studies on Ni–Fe manufactured electrochemically on different substrates have mainly focused on the effect of the H_3BO_3 content on the effectiveness of the ED process, Fe and Ni polarization behaviors and chemical composition of the samples [29, 35–41]. Few researchers (Gangasingh and Talbot [40] and Kashiwa et al. [41]) have addressed the influence of adding H_3BO_3 to the AE on the morphologies of the Ni–Fe films. Moreover, different results concerning the effect of the H_3BO_3 on the surface performance have been reported [40, 41]. Therefore, the influence of the H_3BO_3 content in the AE on the Ni–Fe/ITO thin film samples is of interest. In this paper, we have studied the influence of the H_3BO_3 content in the AE not only on the deposit composition but also on the structural and magnetic properties, morphological characteristics and magnetic domain structure of the electrochemically deposited Ni–Fe/ITO thin film samples.

2. Experimental

Thin films of Ni–Fe samples were deposited from the sulphate based electrolytes including 0.070 M Ni sulphate ($\text{NiSO}_4 \cdot 6\text{H}_2\text{O}$), 0.0045 M Fe sulphate ($\text{FeSO}_4 \cdot 7\text{H}_2\text{O}$) and various H_3BO_3 contents ranging from 0.10 to 0.04 M with an interval of 0.02 M. Apart from these reactants, further additives and complexing agents were not used in the AEs. The manufacturing process was performed by means of a potentiostat/galvanostat (VersaSTAT 3) in a cell consisting of three electrodes (a counter electrode, a reference electrode and a working electrode). A platinum sheet with an area of 150 mm^2 was utilized as a counter electrode. The reference electrode was a saturated calomel electrode (SCE) and an indium tin oxide (ITO) covered glass was served as a working electrode. The sheet-resistance and thickness of the magnetron sputtered ITO-covered glass substrates were $8\text{--}12 \text{ } \Omega/\text{sq}$ and $160\text{--}180 \text{ nm}$, respectively. Prior to ED process of the samples, as a first step of a substrate cleaning process, the ITO-covered glass substrates with a working area of 100 mm^2 were washed in an acetone solution for 10 minutes and then in an ethanol solution for 10 minutes. Subsequently, they were cleaned in deionized water for 15 minutes via an ultrasonic bath. After the substrate cleaning process, the films were electroplated from the AEs with a pH value of 5 ± 0.2 under galvanostatic conditions at ambient temperature of $20 \pm 1 \text{ } ^\circ\text{C}$ by applying a current density of $-20 \text{ mA}/\text{cm}^2$. The thickness of the samples was adjusted to approximately 300 nm by controlling the charge using Faraday's law for all H_3BO_3 contents.

The influence of the H_3BO_3 content in the AE on the crystallite size and crystal structure was explored by a Rigaku Smart LabTM X-ray diffractometer (XRD). The scan was done in the range of $40^\circ\text{--}55^\circ$ with 0.01° steps using a Cu– $\text{K}\alpha$ radiation with $\lambda = 0.15406 \text{ nm}$. To determine the differences in the Fe content of the deposits in atomic percentages (at.%) with respect to the H_3BO_3 content in the AE, an energy dispersive X-ray spectroscopy (EDX) was employed. The impact of the H_3BO_3 content on the magnetic characteristics such as coercivity and magnetic squareness ratio was determined at ambient temperature and pressure using a JDAW–2000D model vibrating sample magnetometer (VSM) by applying the magnetic field along the in-plane direction. The surface morphologies were imaged using a scanning electron microscopy (SEM, Tescan MAIA3 XMU) and an atomic force microscopy (AFM, MultiMode V SPM of Veeco) operating in tapping mode. The roughness parameters were evaluated through the WSxM software package (Version 5.0) [42]. Magnetic domain structure was analyzed by magnetic force microscopy (MFM) operating in lift mode. Prior to zero-field MFM measurements, the CoCr-covered tips were magnetized along the tip axis via a permanent magnet. During MFM imaging, the distance between the film surface and the tip was held at 180 nm not only to increase the magnetic signal but also to decrease the surface contribution.

3. Results and discussion

To see the influence of the H_3BO_3 content on the properties of the Ni–Fe deposits, we produced the Ni–Fe thin films on the ITO substrate from the AEs consisting of Ni and Fe ions and different H_3BO_3 contents. The deposits electrochemically fabricated from the AEs with the H_3BO_3

contents of 0.06, 0.08 and 0.10 M adhered well to the ITO substrate surface without any brittle properties. However, the proper ED process could not be carried out properly when the films were manufactured from the AE containing the H_3BO_3 contents (< 0.06 M). Because, these films showed a brittle feature during manufacturing process. These results are in good agreement with those of former studies documented in the literature [17, 18, 26]. As a consequence, the proper ED processes were established from the AEs composed of 0.06, 0.08 and 0.10 M H_3BO_3 contents.

According to EDX measurements performed for the compositional analysis of the Ni–Fe samples electroplated at various H_3BO_3 contents, there is a very slight increment in the Fe content from 7.2 to 7.8 at.% as the content of the H_3BO_3 in the AE is enhanced from 0.06 to 0.10 M. This result indicates that the impact of the H_3BO_3 content in the AE on the Fe content of the Ni–Fe/ITO thin films is negligible under these experimental conditions. However, different results exist in the literature regarding the impact of the H_3BO_3 content in the AE on the Ni–Fe system. The studies showed that the H_3BO_3 tends to increase the Fe content in the deposit structure [35–37, 39, 40]. In contrast, the films contained smaller Fe content when the H_3BO_3 was present in the AE [38, 41]. These contradictory findings may arise from different parameters applied in the electroplating experiments such as applied current density or deposition potential, substrate type and AE properties, etc.

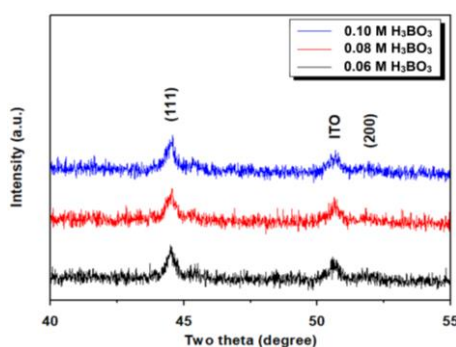


Fig. 1. XRD patterns of the electrochemically prepared Ni–Fe/ITO thin film samples for different H_3BO_3 contents.

The recorded XRD patterns are demonstrated in Fig. 1. The diffraction peaks corresponding to the (111) and (200) crystallographic planes of the face-centered cubic (fcc) phase structure appear on the XRD patterns, reflecting that the films are single phase solid solutions. These results are very good in accordance with those of reported in previous studies [32, 43, 44]. It has been reported that the crystal structure of electrochemically grown Ni–Fe samples at $< 50\%$ Fe composition is fcc [43, 44]. On the other hand, as clearly seen from Fig. 1, the (111) diffraction peak always has a very high intensity compared to the (200) one, indicating the formation of [111] preferred orientation regardless of the H_3BO_3 content. The intensity of the (111) and (200) diffraction peaks does not change appreciably with the H_3BO_3 content. Furthermore, the effect of H_3BO_3 content in the AE on the intensity of the diffraction peak due to the ITO-covered glass is insignificant. This means that the current efficiency (hence the thickness of the Ni–Fe/ITO samples) is not strongly affected by changing the H_3BO_3 content from 0.10 to 0.06 M in the AE, which is in good agreement with the results of previous studies [36, 37, 40]. It was shown that a significant change in the thickness of the Ni–Fe/ITO gives rise to a strong change in the ITO diffraction peak intensity, supporting our results [33].

The crystallite size (CS) was determined using the Scherrer's formula [45]:

$$\text{CS} = [0.9\lambda/B\cos\theta] \times [180/\pi]$$

where CS is the crystallite size, θ is the diffraction angle, λ is the wavelength of Cu–K α radiation and B is the FWHM of the (111) diffraction peak. As given in Table 1, the sizes of the crystallites are found to be in the range of 19.6–20.5 nm. This result shows that the films exhibit nanosized

crystallites and the amount of the H_3BO_3 in the AE does not have a significant impact on the size of the crystallites.

In order to study the magnetic behavior and to investigate the effect of the H_3BO_3 content on the coercivity and magnetic squareness ratio, the in-plane magnetic hysteresis loops were obtained at ambient temperature using a VSM. Figure 2 shows the results of the magnetic measurements for all H_3BO_3 contents. As clearly seen from Fig. 2, all of the films exhibit a ferromagnetic behavior. In addition, the H_3BO_3 content does not play an important role on the coercivity value (Table 1). All of the films exhibit almost the same coercivity values (49 ± 1 Oe). Furthermore, the effect of the H_3BO_3 content on the magnetic squareness ratio is determined to be negligible. As clearly seen from the Table 1, the films exhibit very low and close magnetic squareness ratio values ($\%11 \pm 2$). These very low and close magnetic squareness ratio values reveal not only an insignificant impact of the H_3BO_3 content on the magnetic squareness ratio but also confirm the formation of the magnetization component in the perpendicular direction to the sample plane [46–49]. Moreover, in many different systems, the formation of magnetic stripe domains was attributed to the presence of perpendicular magnetization component [7, 47, 48, 50–57], which is consistent with the results of the MFM measurements presented below.

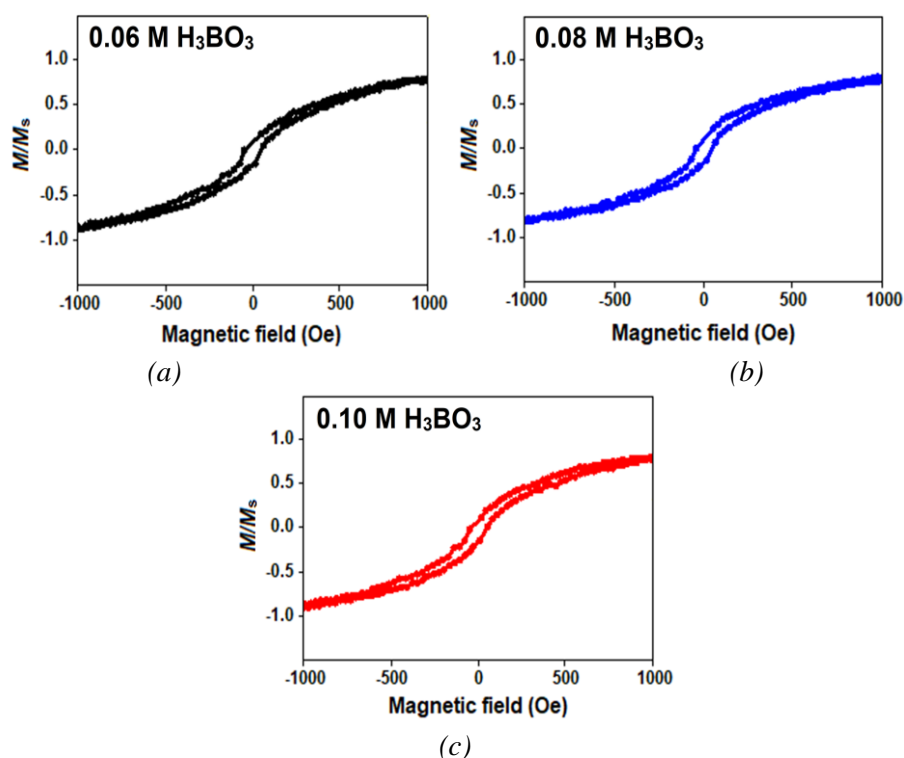


Fig. 2. Room temperature normalized in-plane magnetic hysteresis loops for various H_3BO_3 contents.

The MFM micrographs of the samples are shown in Fig. 3. The MFM micrographs obtained at zero-field state exhibit darker and brighter regions with a weak contrast, indicating the occurrence of the magnetic stripe domain structure with alternating up and down magnetizations irrespective of the H_3BO_3 content in the AE [7, 33, 46, 58–60]. The width of the stripe domains is determined using a two-dimensional Fast Fourier Transform analysis (2D-FFT) of the MFM micrographs. As clearly noticed from Fig. 3, there is no significant difference in the width of the stripe domains of the films deposited from the AEs with various H_3BO_3 contents. All of the films electroplated at different H_3BO_3 contents have quite large magnetic stripe domains with a width of 1.6 ± 0.2 μm . This phenomenon indicates the occurrence of very strong long-range interactions between the particles [60, 61] and the effect of the H_3BO_3 content on the stripe domain width is negligible. Accordingly, it is concluded that the impact of the H_3BO_3 content on the Fe composition, crystallite size, coercivity, magnetic squareness ratio and stripe domain width is

insignificant. However, the same thing cannot be said for the surface morphology. The particle size and surface roughness parameters are noticeably affected by the amount of the H_3BO_3 content in the AE as discussed below.

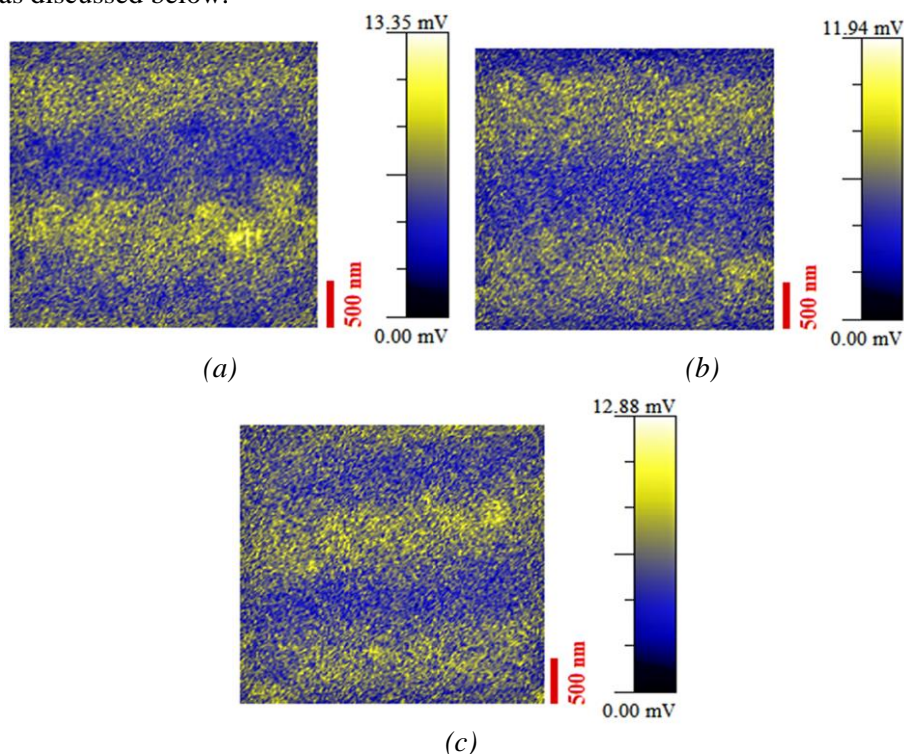


Fig. 3. MFM micrographs obtained at zero-field state over a scan area of $3\ \mu\text{m} \times 3\ \mu\text{m}$ for various H_3BO_3 contents (a) 0.06 M, (b) 0.08 M and (c) 0.10 M, respectively.

The surface morphologies of the electroplated Ni-Fe/ITO thin films imaged through the SEM measurements obtained at low and high magnifications are shown in Fig. 4 for the lowest (0.06 M) and highest (0.10 M) H_3BO_3 contents. The films exhibit a uniform surface structure consisting of nodular particles. However, as can be observed in Fig. 4, the amount of the H_3BO_3 in the AE plays a significant role on the width and density of the nodular particles. It is determined that the film electrochemically deposited from the electrolyte with the lowest H_3BO_3 content of 0.06 M possesses the largest nodular particles in the range of 100 to 400 nm with an average width of ~ 230 nm. However, the film electrochemically grown from the AE containing the highest H_3BO_3 content of 0.10 M exhibits the smallest nodular particles varying between 30 and 150 nm with an average width of ~ 70 nm, resulting the formation of the more compact surface structure relative to other films. Consequently, an enhancement in the H_3BO_3 content in the AE leads to a strong increase in the nucleation density, which was ascribed to the adsorptive interactions of the H_3BO_3 at the electrode surface [19, 20]. Similar effects of the H_3BO_3 content on the surface morphologies have been also reported in electrochemically deposited Ni [19], Zn-Co [20, 22], Co-Cu [23], Ni-Zn [25] and Ni-Fe [41]. However, the study showed that the addition of the H_3BO_3 to the AE does not play a significant role on the surface morphology of electrochemically deposited Ni-Fe on a rotating disk electrode [40]. In the present work, more detailed surface characterization supporting the SEM results was also performed using an AFM and the results are provided below.

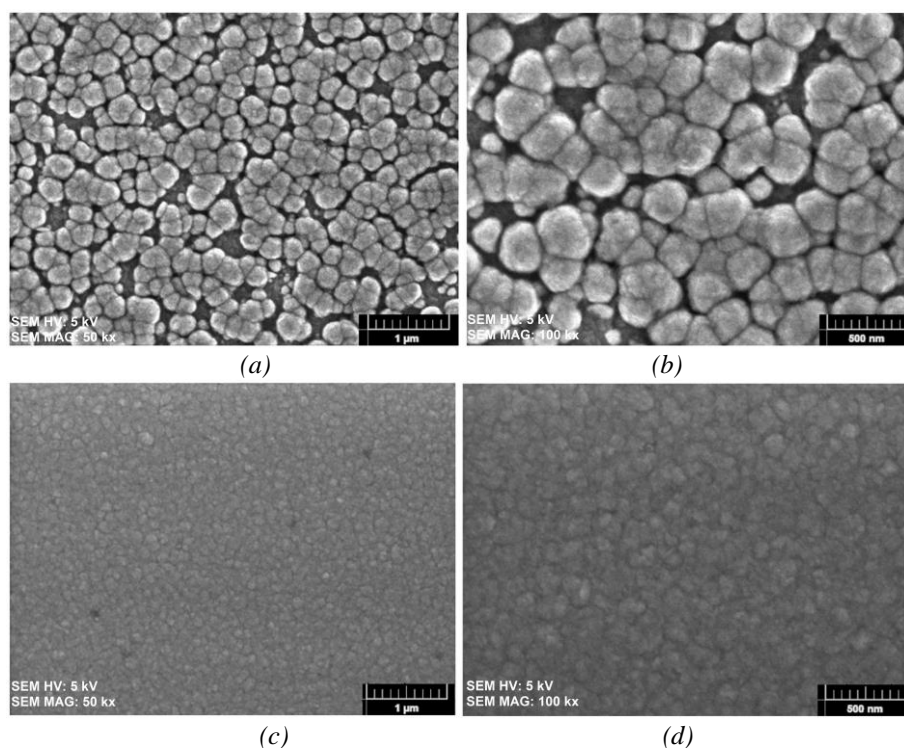


Fig. 4. SEM micrographs for the lowest and the highest H_3BO_3 contents (a) 0.06 M (low-magnification), (b) 0.06 M (high-magnification) (c) 0.10 M (low-magnification) and (d) 0.010 M (high-magnification), respectively.

The obtained three dimensional (3D) AFM micrographs of the samples grown from the AEs with different BA contents are demonstrated in Fig. 5. The images confirm that the films have a surface structure consisting of particles with various sizes. From the 3D AFM micrographs, it is also concluded that increasing H_3BO_3 content in the AE leads to a marked reduction in the particle size, which is in good agreement with the SEM micrographs. In addition, the surface roughness parameters are affected by the differences observed in the size of the particles. The evolution of the roughness parameters, which were derived from the analysis of the AFM micrographs through the WSxM software package [42], is depicted in Fig. 6 depending on the H_3BO_3 content in the AE. The film fabricated from the AE with the H_3BO_3 content of 0.06 M displays the roughest surface with the highest average roughness (Sa) and root mean square roughness (Sq) values. The Sq and Sa values are determined to be 45.9 and 37.9 nm for the film deposited at the H_3BO_3 content of 0.06 M, respectively. Compared to the film electroplated at the H_3BO_3 content of 0.06 M, the film electroplated at the H_3BO_3 content of 0.08 M exhibits significantly lower Sq and Sa values of 6.4 and 5.0 nm, respectively. The lowest Sq and Sa values (4.0 and 3.1 nm, respectively) are obtained for the film fabricated at the highest H_3BO_3 content of 0.10 M, revealing the remarkable influence of the H_3BO_3 content in the AE on the surface performance of the electrochemically deposited Ni-Fe/ITO samples. The structural and morphological properties and magnetic characteristics of the samples are also summarized in Table 1 with respect to the H_3BO_3 content in the AE.

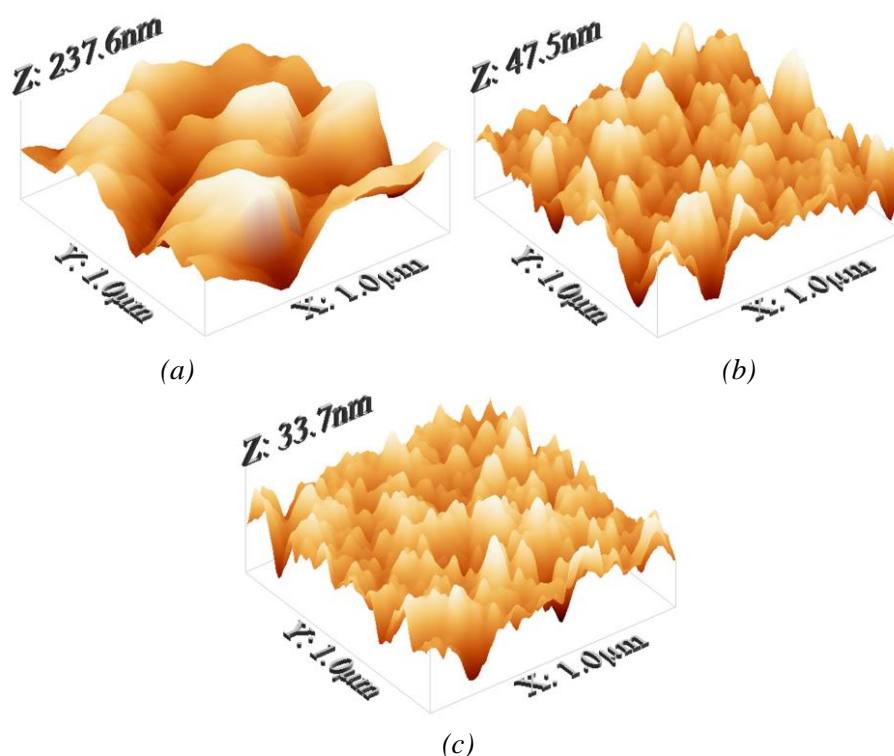


Fig. 5. 3D AFM micrographs for various H_3BO_3 contents (a) 0.06 M, (b) 0.08 M and (c) 0.10 M, respectively.

Overall, this study reveals the negligible effect of the H_3BO_3 content on the crystallite size, Fe content, coercivity, magnetic squareness ratio and magnetic stripe domain width but confirms its key role on the surface quality and proper ED process of the Ni–Fe/ITO samples.

Table 1. The structural and morphological properties and magnetic characteristics for various H_3BO_3 contents.

H_3BO_3 content in the AE (M)	0.06	0.08	0.10
CS (nm)	20.5	19.6	20.4
Average particle size (nm)	~230	~90	Σ70
Sq (nm)	45.9	6.4	4.0
Sa (nm)	37.9	5.0	3.1
Coercivity (Oe)	49	48	50
Magnetic squareness ratio (%)	10	13	11

4. Conclusions

The purpose of this research was to examine the impact of the H_3BO_3 content in the AE on the magnetic characteristics, chemical composition, domain structure, morphological and structural properties of the Ni–Fe/ITO thin film samples. The proper films without brittle properties were electroplated from the AEs with the H_3BO_3 contents of 0.06, 0.08 and 0.10 M. However, the brittle films were obtained at low H_3BO_3 contents (< 0.06 M) under the conditions applied in this study. All of the films displayed the identical Fe and Ni contents (7.5 ± 0.3 at.% Fe and 92.5 ± 0.3 at.% Ni). The fcc structure with the [111] preferred orientation was determined in the deposits. Furthermore, the crystallite size estimated by Scherrer's formula was found to be in the range of 19.6–20.5 nm irrespective of the H_3BO_3 content. The films displayed almost the same

coercivity of 49 ± 1 Oe and very low and close magnetic squareness ratio of $\% 11 \pm 2$. Also, quite large magnetic stripe domains with a width of $1.6 \pm 0.2 \mu\text{m}$ were detected at all H_3BO_3 contents.

However, increasing H_3BO_3 content in the AE gave rise to a noticeable reduction in the average width of the surface particles from about 230 to 70 nm. Moreover, as the content of the H_3BO_3 content in the AE was increased from 0.06 to 0.10 M the Sa and Sq roughness values decreased considerably from 37.9 to 3.1 nm and from 45.9 to 4.0 nm, respectively. Consequently, this research showed that the impact of the H_3BO_3 content in the AE on the crystallite size, chemical composition, coercivity, magnetic squareness ratio and magnetic stripe domain width of the electroplated Ni–Fe/ITO thin film samples is negligible. It was also shown that the amount of the H_3BO_3 in the AE must be controlled for the proper ED process of the Ni–Fe/ITO thin films without brittle properties and to produce samples exhibiting high surface quality characterized by low surface roughness, compact surface structure and small particle size.

Acknowledgements

This work was financially supported by the Scientific Research Projects Commission of Bartın University under the project number 2018–FEN–A–021. The authors would like to thank Çağdaş Denizli for taking AFM and MFM images.

References

- [1] G. Maizza, H. Eom, M. Lee, T. H. Yim, E. Nakagawa, R. Pero, T. Ohmura, *J. Mater. Sci.* **54**, 13378 (2019).
- [2] E. I. Manimaran, K. Antonyraj, E. R. Navaneetha, V. S. Kumar, P. Rajesh, *J. Mater. Sci. Mater. Electron.* **29**, 3715 (2018).
- [3] H. Li, F. Ebrahimi, *Mater. Sci. Eng. A* **347**, 93 (2003).
- [4] S. Arabi, G. Avramovic–Cingara, G. Palumbo, U. Erb, M. Niewczas, *Mater. Sci. Forum* **706-709**, 1642 (2012).
- [5] N. Myung, *Bull. Korean Chem. Soc.* **22**, 994 (2001).
- [6] T.-R. Lee, L. Chang, C.-H. Chen, *Surf. Coat. Technol.* **207**, 523 (2012).
- [7] L. X. Phua, N. N. Phuoc, C. K. Ong, *J. Alloys Compd.* **520**, 132 (2012).
- [8] H. Nakano, M. Matsuno, S. Oue, M. Yano, S. Kobayashi, H. Fukushima, *Mater. Trans.* **45**, 3130 (2004).
- [9] V. Torabinejad, M. Aliofkhaezaei, S. Assareh, M. H. Allahyarzadeh, A. S. Rouhaghdam, *J. Alloys Compd.* **691**, 841 (2017).
- [10] X. Hou, S. Liu, J. Li, S. Yang, B. Guo, *Mater. Manufact. Process.* **31**, 62 (2016).
- [11] X. Su, C. Qiang, *Bull. Mater. Sci.* **35**, 183 (2012).
- [12] B. Subramanian, K. Govindan, V. Swaminathan, M. Jayachandran, *Trans. Inst. Metal Finish.* **87**, 325 (2009).
- [13] Y. Cao, G. Y. Wei, H. L. Ge, X. F. Meng, *Surf. Eng.* **30**, 97 (2014).
- [14] Á. Llavona, L. Pérez, M. C. Sánchez, V. de Manuel, *Electrochim. Acta* **106**, 392 (2013).
- [15] B. E. B. Al-Jumaili, Z. A. Talib, A. Ramizy, A. I. Aljameel, H. Baqiah, N. M. Ahmed, S. B. Paiman, J. Y. C. Liew, H. K. Lee, *Dig. J. Nanomater. Biostruct.* **16**, 297 (2021).
- [16] J. Vazquez-Arenas, L. Altamirano-Garcia, T. Treeratanaphitak, M. Pritzker, R. Luna-Sanchez, R. Cabrera-Sierra, *Electrochim. Acta* **65**, 234 (2012).
- [17] Y. Tsuru, M. Nomura, F. R. Foulkes, *J. Appl. Electrochem.* **32**, 629 (2002).
- [18] Y. Wu, D. Chang, D. Kim, S.-C. Kwon, *Surf. Coat. Technol.* **173**, 259 (2003).
- [19] M. Šupicová, R. Rozik, L. Trnková, R. Oriňáková, M. Gálová, *J. Solid State Electrochem.* **10**, 61 (2006).
- [20] C. Karwas, T. Hepel, *J. Electrochem. Soc.* **136**, 1672 (1989).
- [21] C. E. Dávalos, J. R. López, H. Ruiz, A. Méndez, R. A.-López, G. Trejo, *Int. J. Electrochem. Sci.* **8**, 9785 (2013).
- [22] I. H. Karahan, H. A. Çetinkara, *Trans. Inst. Met. Finish.* **89**, 99 (2011).

- [23] S. S. Abd El-Rehim, S. M. Abd El-Wahab, S. M. Rashwan, Z. M. Anwar, *J. Chem. Technol. Biotechnol.* **75**, 237 (2000).
- [24] C. Lupi, D. Pilone, *Miner. Eng.* **14**, 1403 (2001).
- [25] C. Karwas, T. Hepel, *Alloys, J. Electrochem. Soc.* **135**, 839 (1988).
- [26] M. Holm, T. J. O'Keefe, *J. Appl. Electrochem.* **30**, 1125 (2000).
- [27] A. Dolati, M. Ghorbani, A. Afshar, *Surf. Coat. Technol.* **166**, 105 (2003).
- [28] A. Saedi, M. Ghorbani, *Mater. Chem. Phys.* **91**, 417 (2005).
- [29] N. Zech, D. Landolt, *Electrochim. Acta* **45**, 3461 (2000).
- [30] R. Oriňáková, A. Turoňová, D. Kladeková, M. Gálová, R. M. Smith, *J. Appl. Electrochem.* **36**, 957 (2006).
- [31] H. Deligianni, L. T. Romankiw, *Electrochem. Soc. Proc.* **90-98**, 407 (1990).
- [32] U. Sarac, M. Kaya, M. C. Baykul, *Turk. J. Phys.* **41**, 536 (2017).
- [33] D. Cao, Z. Wang, E. Feng, J. Wei, J. Wang, Q. Liu, *J. Alloys Compd.* **581**, 66 (2013).
- [34] U. Sarac, M. Kaya, M. C. Baykul, *Dig. J. Nanomater. Biostruct.* **16**, 51 (2021).
- [35] K.-M. Yin, B.-T. Lin, *Surf. Coat. Technol.* **78**, 205 (1996).
- [36] J. Horkans, *J. Electrochem. Soc.* **128**, 45 (1981).
- [37] W. C. Grande, J. B. Talbot, *J. Electrochem. Soc.* **140**, 669 (1993).
- [38] V. C. Kieling, *Surf. Coat. Technol.* **96**, 135 (1997).
- [39] K.-M. Yin, S.-L. Jan, C.-C. Lee, *Surf. Coat. Technol.* **88**, 219 (1997).
- [40] D. Gangasingh, J. B. Talbot, *J. Electrochem. Soc.* **138**, 3605 (1991).
- [41] Y. Kashiwa, N. Nagano, T. Takasu, S. Kobayashi, K. Fukuda, H. Nakano, *ISIJ Int.* **59**, 514 (2019).
- [42] I. Horcas, R. Fernández, J. M. G. Rodríguez, J. Colchero, J. G. Herrero, A. M. Baro, *Rev. Sci. Instrum.* **78**, 013705 (2007).
- [43] C.-W. Su, E.-L. Wang, Y.-B. Zhang, F.-J. He, *J. Alloys Compd.* **474**, 190 (2009).
- [44] N. V. Myung, K. Nobe, *J. Electrochem. Soc.* **148**, C136 (2001).
- [45] J. Wang, W. Lei, Y. Deng, Z. Xue, H. Qian, W. Liu, X. Li, *Surf. Coat. Technol.* **358**, 765 (2019).
- [46] X. Zhou, Z. Wang, S. Ge, D. Wang, J. Yu, D. Yao, *Phys. Status Solidi A* **211**, 2839 (2014).
- [47] F. Zhang, S. Ge, Z. Wang, X. Zhou, G. Wang, Z. Yu, F. Li, *J. Alloys Compd.* **506**, 109 (2010).
- [48] A. Gayen, G. Kr. Prasad, K. Umadevi, J. A. Chelvane, P. Alagarsamy, *J. Magn. Magn. Mater.* **462**, 29 (2018).
- [49] N. Sulițanu, F. Brînză, *J. Optoelectron. Adv. Mat.* **5**, 421 (2003).
- [50] M. Coisson, G. Barrera, F. Celegato, P. Tiberto, *Appl. Surf. Sci.* **476**, 402 (2019).
- [51] S. W. Fackler, M. J. Donahue, T. Gao, P. N. A. Nero, S.-W. Cheong, J. Cumings, I. Takeuchi, *Appl. Phys. Lett.* **105**, 212905 (2014).
- [52] S. Voltan, C. Cirillo, H. J. Snijders, K. Lahabi, A. García-Santiago, J. M. Hernández, C. Attanasio, J. Aarts, *Phys. Rev. B* **94**, 094406 (2016).
- [53] X. Zhou, D. Yao, W. Xie, J. Wei, G. Xu, *J. Alloys Compd.* **533**, 58 (2012).
- [54] L. Sun, J. H. Liang, X. Xiao, C. Zhou, G. Chen, Y. Huo, Y. Z. Wu, *AIP Adv.* **6**, 056109 (2016).
- [55] J. Jiao, T. Wang, T. Ma, Y. Wang, F. Li, *Nanoscale Res. Lett.* **12**, 21 (2017).
- [56] A. Masood, P. McCloskey, C. Mathúna, S. Kulkarni, *AIP Adv.* **7**, 055208 (2017).
- [57] L. Raghavan, S. Ojha, I. Sulania, N.C. Mishra, K.M. Ranjith, M. Baenitz, D. Kanjilal, *Thin Solid Films* **680**, 40 (2019).
- [58] M. Cichomski, W. Szmaja, *Appl. Phys. A* **102**, 339 (2011).
- [59] X. Zhou, D. Yao, C. Hou, R. Chen, H. Shen, *J. Magn. Magn. Mater.* **438**, 1 (2017).
- [60] Ç. Denizli, U. Saraç, M. C. Baykul, *J. Mater. Sci. Mater. Electron.* **31**, 4279 (2020).
- [61] X. Sun, Z. Li, F. Xu, Y. Wang, *J. Alloys Compd.* **656**, 812 (2016).